Applied Surface Science, 434, 1300–1310 (2018)

Pressure resistance of copper benzene-1,3,5-tricarboxylate – carbon aerogel composites

Andrea Domán[a], Balázs Nagy[a], Laura P. Nichele[a,b], Dávid Srankó[c], János Madarász[d], Krisztina László[a]*
[a]Department of Physical Chemistry and Materials Science, Budapest University of Technology and Economics, 1521 Budapest, Hungary
[b]Department of Chemical Engineering, University of Sao Paulo, Lorena, Brazil
[c]Institute for Energy Security and Environmental Safety, Centre for Energy Research, Hungarian Academy of Sciences, Budapest, Hungary
[d]Department of Inorganic and Analytical Chemistry, Budapest University of Technology and Economics, 1521 Budapest, Hungary

*Corresponding author
Krisztina László:
E-mail: klaszlo@mail.bme.hu, Phone: +36-1-463-1893, Fax: + 36-1-463-3767

Author email addresses:
János Madarász: madarasz@mail.bme.hu
Andrea Domán: doman.andrea@mail.bme.hu
Balázs Nagy: balazs.nagy@mail.bme.hu
Dávid Srankó: sranko.david@energia.mta.hu
Laura P. Nichele: lauranichele@alunos.eel.usp.br

Abstract
The protective effect of a resorcinol – formaldehyde based carbon aerogel (CA) support was compared in two different forms of the hybrid made of copper benzene-1,3,5-tricarboxilate (HKUST-1) and CA. HKUST-1:CA with identical mass ratio (1:1). HKUST-1+CA is a physical mixture while in HKUST-1@CA the metal organic framework (MOF) crystals were grown on CA under solvothermal conditions. The effect of water vapour and the external pressure (25 - 200 bar) was investigated.
TG/DTG data show that the prehistory of the samples has a strong influence on their thermal behaviour and nitrogen data suggest that part of the MOF grows in the wider pores of the HKUST-1@CA sample. Although there are no dramatic differences in the water adsorption isotherms, the physical mixture is slightly more proficient. In dry samples under compression the crystalline structure of the free HKUST-1 is well conserved. The nanoscale structure of the hybrids is sensitive to applied pressure and formation of mesopores of wide size distribution occurs. No significant difference was found between the corresponding CH_4 adsorption isotherms of the composite samples, either in the as-prepared samples or after compression at 100 bar. After being exposed to high external pressure the CH_4 uptake seems to be governed by the MOF.

Keywords: gas storage, MOF, HKUST-1, water vapour, methane

1. Introduction

Natural gas has a huge potential as alternative fuel owing to its moderately low carbon dioxide emission, but its effective and safe storage is still a challenge. Adsorptive gas storage could be the solution to this problem, but a suitable adsorbent is required [1]. Metal organic frameworks (MOFs) are a relatively a new class of materials with outstandingly large adsorption capacity. MOFs are composed of multivalent metal ions or clusters linked together by organic ligands, thereby creating an open framework with an ordered and permanent pore structure. Owing to these properties MOFs are at present the most promising materials in gas storage applications. Their mechanical stability, however, is poorer than that of traditional adsorbents [2].

Copper benzene-1,3,5-tricarboxilate (Cu_3BTC_2) is one of the most widely investigated MOFs. It is also commercially available as Basolite® C 300. Its three-dimensional network can adsorb an outstandingly large amount of methane, the main component of natural gas. Notably, they met the US DoE target (180 times their own volume at 35 bar) established for natural gas storage [3, 4]. This MOF was first reported in 1999 by Chui et al. as HKUST-1 (Hong Kong University of Science and Technology), who used solvothermal synthesis to prepare the light blue octahedral crystals [5]. Its network structure is built from copper(II) cations and benzene-1,3,5-tricarboxylate anions (BTC) to form a neutral net of interconnected micropores. In its paddle-wheel secondary building unit, four carboxylate groups of four BTC ligands link together two copper ions. In this structure, each copper ion has an unsaturated binding site. In the solvothermal synthesis these binding sites are occupied and the pores fill with solvent molecules, thereby reducing the free volume and the adsorption capacity for the gas to be stored. Removal of these guest molecules is necessary before implementing adsorption [1].

Generally, for easier handling, industrial adsorbents are employed preferentially as pellets or monoliths. The compression step is intended to reduce the space between individual crystals without destroying their structure and if possible to increase the adsorption capacity. In many cases, it has been reported that application of high external pressure to MOFs can result in anomalous mechanical behaviour [6, 7].

In order to investigate how high pressure treatment influences the sorption behaviour of the MOF material HKUST-1 was exposed to high hydrostatic pressure in a diamond anvil cell (DAC) device surrounded by a hydrostatic liquid [8-10]. The pressure was varied in the range 0-80000 bar. It was found that the HKUST-1 framework exhibited a clear transition between two distinct regions of nearly linear compressibility depending on the hydrostatic liquid. In the first region, the applied pressure forced the hydrostatic medium into the pores, causing the sample to expand initially. The framework is then much more resistant to compression. A transition pressure, which depends on the size of the molecules of the hydrostatic liquid entering the pores, occurred between 8000 and 22000 bar. In the second region, the pore filling behaviour transforms into pore discharging, where the high pressure squeezes the solvent out of the pores, thus dramatically decreasing the volume. In the absence of hydrostatic liquid, or when a non-penetrating hydrostatic medium is applied, direct compression of the framework occurs.

The most common response to external pressure is amorphisation. Investigations into the effect of the external pressure include the effect on the structure, adsorption performance and density of HKUST-1. Compression with 0.03 – 5 ton resulted in a loss of the nitrogen adsorption capacity and crystallinity, while bulk density concurrently increased [11]. The appearance of a hysteresis loop in the nitrogen adsorption isotherm after compression indicates the formation of mesopores. Using IR spectroscopy and XRD measurements De Coste et al. after compression with 70 and 700 bar, respectively, demonstrated that the reason of this phenomenon is a physical transformation [12].

The use of HKUST-1 for natural gas (NG) storage however, raises another question, namely the effect of impurities on its integrity (Table 1) [13]. Although water is not listed in this table, it is one of the most critical component from the point of view of HKUST-1 [14-16].

Table 1 Typical components of the natural gas [13]

Methane	CH_4	70-90%
Ethane	C_2H_6	0-20%
Propane	C_3H_8	
Butane	C_4H_{10}	
Carbon Dioxide	CO_2	0-8%
Oxygen	O_2	0-0.2%
Nitrogen	N_2	0-5%
Hydrogen sulphide	H_2S	0-5%
Rare gases	A, He, Ne, Xe	trace

The chemical and mechanical stability of MOFs as well as their resistance to wet environment may be improved in their composites [17]. With mechanically more stable materials such as activated carbons it is possible to reduce the mechanical vulnerability of MOFs. It has also been reported that various (Maxsorb pellet, Westvaco SA-30 carbon powder, activated carbon fibre from Osaka Gas Co. or a lab-made a mesophase pitch-based) activated carbons are much more resistant to compression than HKUST-1. Their nitrogen adsorption capacity showed no significant change under high pressure (0-4120 bar) [18, 19]. HKUST-1 crystals were successfully grown within the pores of the petroleum-pitch activated carbon, thus improving their mechanical resistance. The activated carbon was added to the precursor solution of HKUST-1 prior to the solvothermal synthesis. The nitrogen adsorption capacity of the resulting composite material was not influenced by pelletization under 0.5 - 1.5 tons, and the morphological deformation was negligible [20].

The textural and chemical characteristics of carbon aerogels, which are simultaneously micro-, meso- and macroporous, predispose them as thermal and phonic insulators, electric double layer and super capacitors, chromatography packing, adsorbents, etc. [21]. These materials, like other high surface area materials, are also often used as catalyst supports [22 - 24]. The space between their typically spherical carbon beads is large enough to host particles, e.g., titania, carbon nanoparticles such as graphene derivatives, carbon nanotubes or nanohorns, etc. [25 - 28] or enzymes and cells [29, 30].

This study focuses on the protective impact of resorcinol – formaldehyde based carbon aerogel. HKUST-1 – carbon aerogel composites of identical mass ratio were prepared as i) a physical mixture (HKUST-1+CA), and ii) by synthesizing HKUST-1 in the presence of the aerogel (HKUST-1@CA), similarly to [20]. Each component, as well as the composites, was characterized and their water vapour adsorption was measured. The effect of external pressure was monitored by powder XRD and nitrogen adsorption. The influence of pressure on the gas storage performance was tested by atmospheric methane adsorption at 0 °C.

2. Experimental

2.1. Sample preparation

The resorcinol – formaldehyde based carbon aerogel was prepared by carbonizing the polymer aerogel formed from the resorcinol-formaldehyde polycondensation reaction [31, 32]. The surface of the powdered carbon aerogel was altered from basic to acidic by oxidation with nitric acid. After thorough washing with deionized water the sample was dried at 110 °C. This oxidized sample was denoted as CA. HKUST-1 ($C_{18}H_6Cu_3O_{12}$, Mw 604.87) was synthesized under solvothermal conditions after Wang et al. [33] at 80 °C [34]. The turquoise crystals obtained were filtered and thoroughly washed with ethanol, then dried in air at ambient temperature. The samples were stored in a sealed vial in a desiccator over freshly activated silica. The fine crystalline material was used without further crushing or grinding.
Binary samples of approximately identical gravimetric composition (HKUST-1:CA = 1:1), obtained by two different routes, were used in the experiments. For the "chemical" composite (HKUST-1@CA) CA soaked in the aqueous solution of $Cu(NO_3)_2$ was added to the above described precursor solution prior to the solvothermal process. For the "physical" mixture (HKUST-1+CA), CA and HKUST-1 materials were thoroughly homogenized.

2.2. Compression
An OL57 hydraulic press (Manfredi, Italy) was used for sample compression. 100 mg of sample was placed in a 13 mm diameter sample holder and kept at the required pressure (25 bar, 50 bar, 100 bar and 200 bar) for 10 minutes. The compressed samples were designated by sample name_applied pressure. HKUST-1_200 thus refers to HKUST-1 compressed at 200 bar.

2.2. Characterization
The powder X-ray diffraction (XRD) was measured in the range 2Θ = 4–84° with an X'pert Pro MPD (PANanalytical Bv., The Netherlands) X-ray diffractometer using an X'celerator type detector and Cu K_α radiation with a Ni filter foil (λ = 1.5408 Å) on a 'zero-background Si-single crystal' sample holder. Phase identification was assisted by the Search&Match algorithm of HighScore Plus (PANanalytical Bv.) software, based on either the international Powder Diffraction File (PDF4+, Release 2015, International Centre of Diffraction Data, ICDD, Pennsylvania, USA), or The Cambridge Structural Database (CSD-Enterprise, version 5.37, Cambridge Crystallographic DataCentre, CCDC [35]) using the built-in powder pattern generator algorithm of Mercury program [36]. For this measurement, non-activated samples were used.
Thermal analysis was performed using a simultaneous TG/DTA apparatus (STD 2960 Simultaneous DTA-TGA, TA Instruments Inc., USA). The heating rate was 10 °C min^{-1}, with a dry air flow of 130 cm^3 min^{-1}. Approximately 10 mg of sample were placed in an open Pt crucible.
Surface composition was determined by X-ray photoelectron spectroscopy (XPS) performed by a KRATOS XSAM 800 XPS machine equipped with an atmospheric reaction chamber. Al Kα characteristic X-ray line. 40 eV pass energy (energy steps 0.1 eV) and FAT mode were applied for recording the XPS lines of *Cu 2p, Cu LMM, O 1s* and *C 1s*. *C 1s* binding energy at 284.8 eV was used as reference for charge compensation. The surface concentrations of the elements were calculated from the integrated intensities of the XPS lines using sensitivity factors given by the manufacturer.
Nitrogen adsorption/desorption isotherms were measured at -196 °C by a NOVA 2000e (Quantachrome, USA) volumetric computer-controlled surface analyzer. The samples were outgassed in vacuum at 180 °C (activation). The apparent surface area S_{BET} was calculated using the Brunauer–Emmett–Teller (BET) model [37]. The total pore volume V_{tot} was derived from the amount of vapour adsorbed at relative pressure $p/p_0 \rightarrow 1$, assuming that the pores are filled with liquid adsorbate. The micropore volume $V_{microN2}$ was derived from the Dubinin–Radushkevich (DR) plot [38]. The pore size distribution was calculated using the Barret-Joyner-

Halenda (BJH) model [39]. Transformation of the primary adsorption data and pore size analysis were performed with the QuantachromeASi Qwin software (version 3.0).

2. Water vapour adsorption

Water vapour adsorption/desorption isotherms were measured at 20 °C by a NOVA 2000e (Quantachrome, USA) volumetric computer-controlled surface analyzer. The samples were outgassed in vacuum at 180 °C (activation).

2.4. Methane adsorption

Methane adsorption/desorption isotherms were measured at 0 °C by AUTOSORB-1 (Quantachrome, USA) volumetric computer-controlled surface analyzer. Prior to the measurements the samples were outgassed at 180 °C (activation). The total pore volume V_{tot} was derived from the amount of vapour adsorbed at relative pressure $p/p_0 \rightarrow 1$, assuming that the pores are filled with liquid adsorbate. Transformation of the primary adsorption data was performed with the QuantachromeASi Qwin software (version 3.0).

3. Results and discussion

3.1. Characterisation of the uncompressed materials

Figure 1 shows SEM micrographs of the pristine MOF and the porous carbon aerogel. The as-prepared freely grown HKUST-1 forms light blue octahedral crystals (Fig. 1a) [40]. To obtain octahedral HKUST-1 crystals grown on the surface of the CA the originally basic surface of the carbon aerogel had to be converted to acidic. It was reported earlier that acidic surface groups are advantageous for HKUST-1 formation [17].

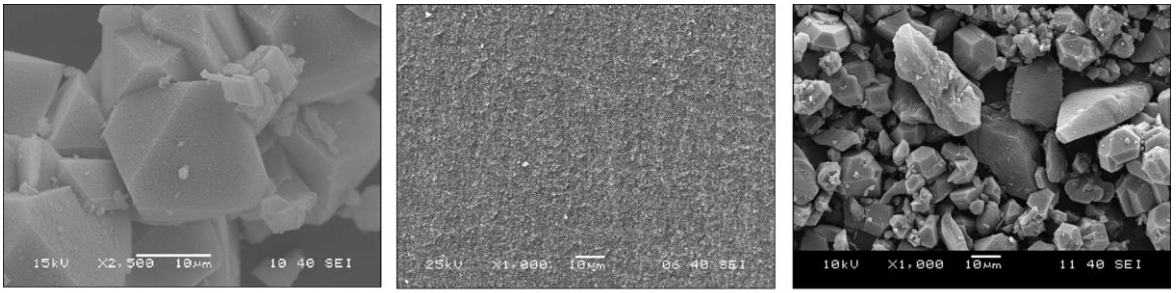

a **b** **c**

Fig. 1 Scanning electron micrographs of the HKUST-1 (a), the carbon aerogel (b) and HKUST-1@CA (c)

The diffraction profile of the composites confirms the presence of the HKUST-1 crystals (Fig. 2). In the composite samples the peak positions do not change, with only a slight peak broadening being observed, probably due to the presence of the amorphous CA. The peak positions of our samples agree well with the reference patterns of $Cu_3(BTC)_2$ from both the international CSD single crystal and PDF-4+ powder diffraction databases (FIQCEN [41], DOTSOV42 [42] and PDF 00-062-1183 [43], PDF 00-64-0936 [44], and PDF 00-065-1028 [45]).

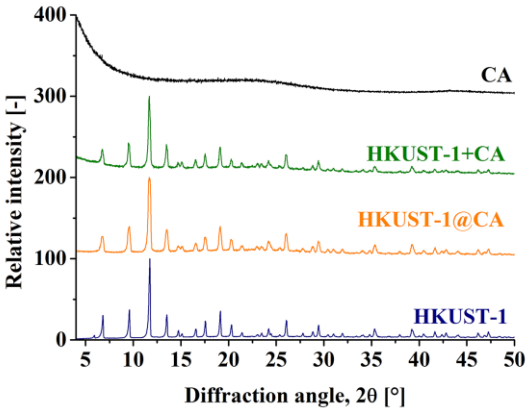

Fig. 2 Powder XRD profile of the non-activated samples: HKUST-1, HKUST-1@CA, HKUST-1+CA and CA. (Each spectrum is normalized with respect to its highest count (100%).

The chemical nature of the copper in the HKUST-1@CA composite samples was examined by XPS (Fig. 3). The Cu2p peak shows shake up satellites, which are a clear sign of Cu^{2+}. These anchored ions are not crystalline, i.e., they cannot be detected by XRD. Due to the heterogeneous charge up of the sample, correct deconvolution of the peaks is not possible. No chemical relation between the Cu atoms and the CA surface was identified, i.e., in this respect the HKUST-1@CA sample appears to resemble a physical mixture of HKUST-1 and CA rather than a chemically integrated material.

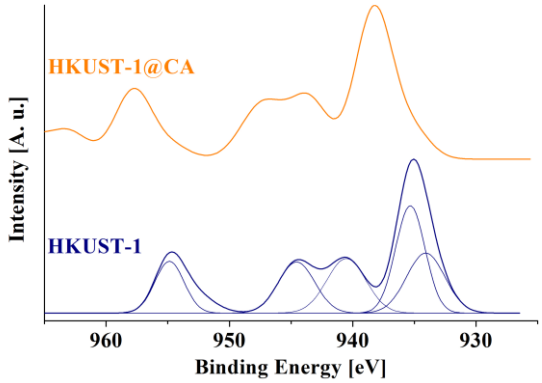

Fig. 3 Cu 2p XPS spectra of HKUST-1(a) and the HKUST-1@CA (b) samples

The porous structure of the two composites are very similar (Fig. 4). HKUST-1 has a Type I isotherm [46], typical of microporous materials. The pore filling mechanism is indicated by the nitrogen adsorption, which is fully reversible. The isotherm of CA, of Type IV, reveals the presence of micro- and relatively wide mesopores. CA is clearly recognizable in the isotherms of the composite samples. The pore size distribution of the uncompressed HKUST-1@CA and HKUST-1+CA, as will be shown later in Figures 10b and 11b, respectively, shows mesopores with a typical diameter of 30 nm in both composites. Table 2 lists the numerical characteristics deduced from the isotherms. A set of theoretical data (X_{theor}) was also created for the composite samples assuming that the adsorption capacity of the components is additive. Strictly speaking, for the exclusively microporous HKUST-1, the BET model can be employed only as an approximation. We use this apparent area as a benchmark to characterize our systems.

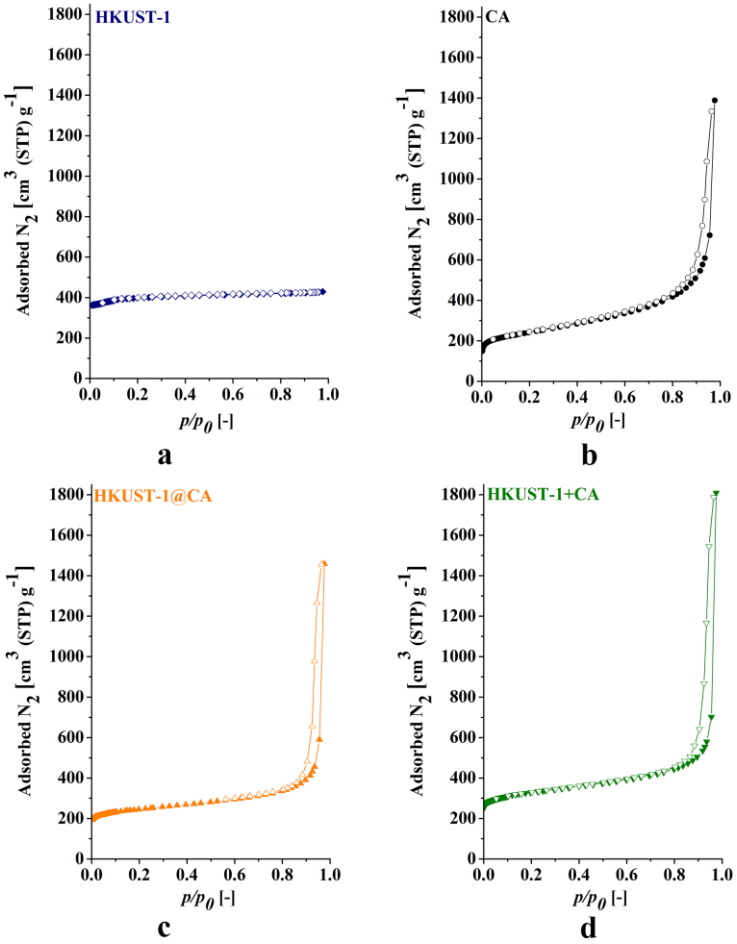

Fig. 4 Low temperature (-196 °C) nitrogen adsorption isotherms of HKUST-1 (a), CA (b), HKUST-1@CA (c) and HKUST-1+CA (d) samples
Full symbols: adsorption, open symbols: desorption branch

Table 2 Data deduced from low temperature (-196 °C) nitrogen adsorption measurements and calculated theoretical data

Sample	Measured X_{meas}			Theoretical* X_{theor}		
	S_{BET} $m^2\ g^{-1}$	$V_{microN2}$ $cm^3\ g^{-1}$	V_{tot} $cm^3\ g^{-1}$	S_{BET} $m^2\ g^{-1}$	$V_{microN2}$ $cm^3\ g^{-1}$	V_{tot} $cm^3\ g^{-1}$
HKUST-1	1557	0.58	0.66	-	-	-
CA	873	0.35	2.2	-	-	-
HKUST-1@CA	923	0.35	2.3	1242	0.47	1.4
HKUST-1+CA	1236	0.47	2.8	1207	0.46	1.4

*Corresponding theoretical values X_{theor} calculated from the corresponding measured data X_{meas} as $X_{theor} = \frac{m_{HKUST-1} X_{HKUST-1meas} + m_{CA} X_{CAmeas}}{m_{HKUST-1} + m_{CA}}$. $m_{HKUST-1}$ and m_{CA} are the mass of the solvent free HKUST-1 and dry CA, respectively

While the calculated data of HKUST-1+CA are very close to the measured values, HKUST-1@CA shows a more complex feature. The isotherm of HKUST-1@CA is similar to CA (Fig. 4) in the low p/p_0 range, but the slope in the mesoporous range is less steep than that of the host aerogel alone. The contribution of HKUST-1 to the BET area is much lower than the theoretical

value. These observations imply that HKUST-1 crystals also may grow in the mesopores of the CA, thus reducing the free mesopore volume.
The difference between the two composite samples is more obvious in their thermal behaviour (Fig. 5 and Table S1). Already, simple inspection of the corresponding curves (Fig. 5c and d) shows that the MOF confined within the pores has a substantial impact on the thermal behaviour of the CA.

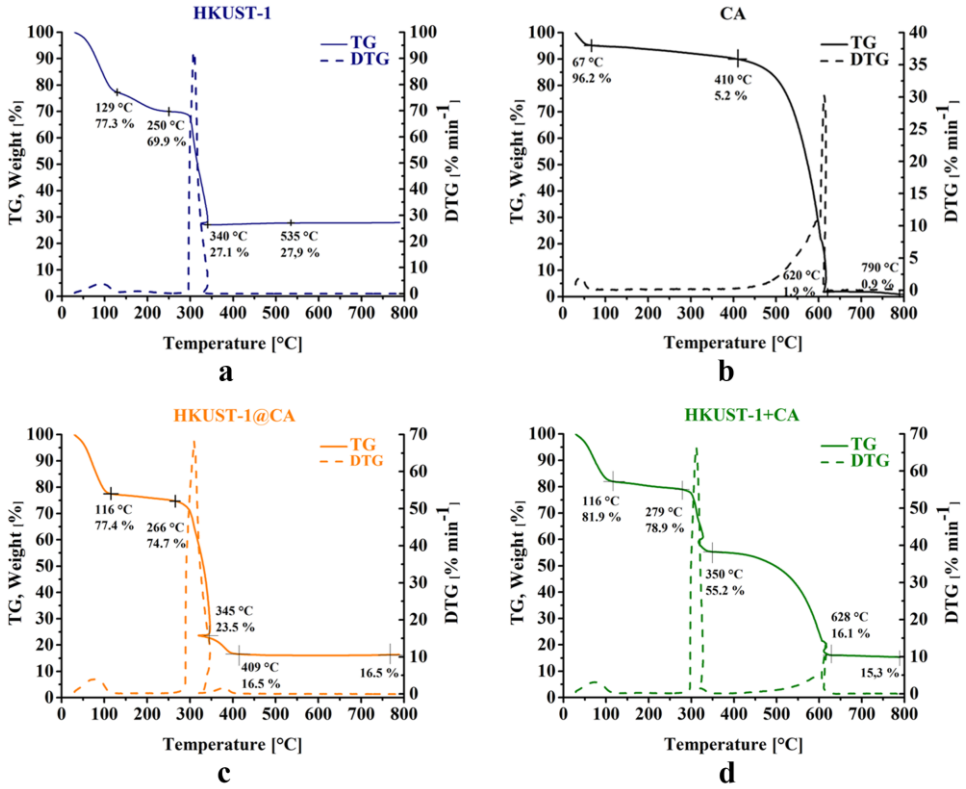

Fig. 5 TG (solid line) and DTG (dotted line) signals of HKUST-1 (a), CA (b), HKUST-1@CA (c) and HKUST-1+CA (d) samples in air (heating rate: 10 min sec^{-1})

CA exhibits three characteristic regions corresponding to i) the loss of adsorbed water, ii) decomposition of surface groups and iii) combustion. The behaviour of the binary samples up to 270 - 280 °C is similar. Above that temperature the difference becomes substantial. In HKUST-1@CA oxidative decomposition of the two components intervenes and the process ends by 410 °C, much below the temperature of the combustion step of pristine CA. As at least part of the HKUST-1 develops within the pores of CA, the evolving gases cannot easily leave the pores and their residence is time long enough to react with the CA. On the other hand, two distinct steps are observable in the HKUST-1+CA, which correspond respectively to the practically independent thermal degradation of the organic ligands of HKUST-1 (- 23.7 % loss) around 320 °C, and to the oxidative decomposition of CA (-39.1 %) above 410 °C. The slight mass increase following the sharp thermal decomposition originates from the transformation of Cu_2O to CuO. It can be used to confirm the stoichiometric composition of HKUST-1 and to estimate the HKUST-1 content of the binary samples [34]. Thus, the HKUST-1 content estimated from the mass of the corresponding residues at 800 °C was found to be very close to the value expected from the preparation conditions (~39 %).
The effect of the CA support on sensitivity to water was tested on samples after preheating at a temperature where all the liquids filling the pores are removed (Fig. 6). The polar HKUST-1 adsorbed about twice as much water as CA, and its binding sites of different strengths are clearly recognizable in the adsorption isotherm [15]. As expected, the interaction between the water

molecules and the HKUST-1 is much stronger than in the case of CA, as reflected in the initial slope of the isotherms. The adsorption/desorption process is irreversible, water molecules being retained in the pores in both pure samples. In both composite samples, the polar character of the MOF defines the shape of the isotherms. The presence of CA reduces the water adsorption capacity, and in HKUST-1+CA this effect is more pronounced. The different binding sites are still distinguishable and the inflections occur at the same p/p_0 values, but the shape of the isotherms is slightly different.

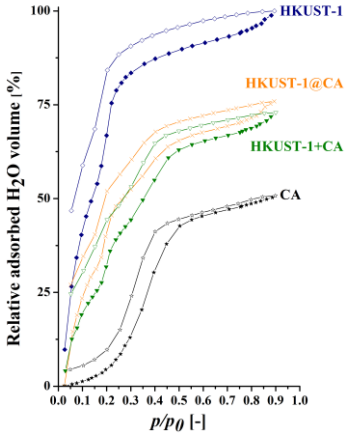

Fig. 6 Water vapour adsorption isotherms of HKUST-1, CA, HKUST-1@CA and HKUST-1+CA samples. The maximum adsorption of HKUST-1 was set to 100 %.

3.2. Influence of the external pressure

The stability of the MOF against external pressure and the potential protective effect of the carbon support were studied up to 200 bar without thermal pre-treatment. Chapman et al., who studied the HKUST-1 in a DAC, reported that applying compression in the 8 - 22 kbar range the hydrostatic liquid enters the pores, while at higher pressure pore emptying occurred [10]. In our case, where no hydraulic medium was applied, at pressures upwards of 100 bar the surface of the pure HKUST-1 discs seemed wet when the hydraulic press was opened. After a few seconds, the moisture disappeared into the pores. The difference in the observed pressures might be explained by the significantly different experimental conditions. With the composite samples, we did not observe such wetting behaviour.

3.2.1. Offline XRD study of pellets compressed by different loads

The diffraction profiles of the compressed samples are compared in Figure 7. Investigating the pressure dependence of the diffraction profile of HKUST-1 *in situ* in DAC observed no significant change in the diffraction profile until 4 kbar [10]. Under our different experimental conditions, our results were different. Although in the freely grown HKUST-1 part of the diffraction profile is still recognizable after compression at 200 bar, structural changes are already observable at 25 bar (Fig. 7a). The peak broadening and increasing base line indicate partial amorphisation of the structure at the nanometre scale. The position of the peaks shifts slightly to larger angles, implying decreased interplanar distance and shortened bond lengths. The two broad bumps (2Θ = 22.9; 43.1 °) of amorphous CA could be the sign of limited structural regularity. Both composite samples show poorer resistance than their individual components. The structure of HKUST-1 disappears in HKUST-1@CA at 50 bar and in HKUST-1+CA at 100 bar, which implies that the physical mixture offers slightly better resistance to pressure than the composites.

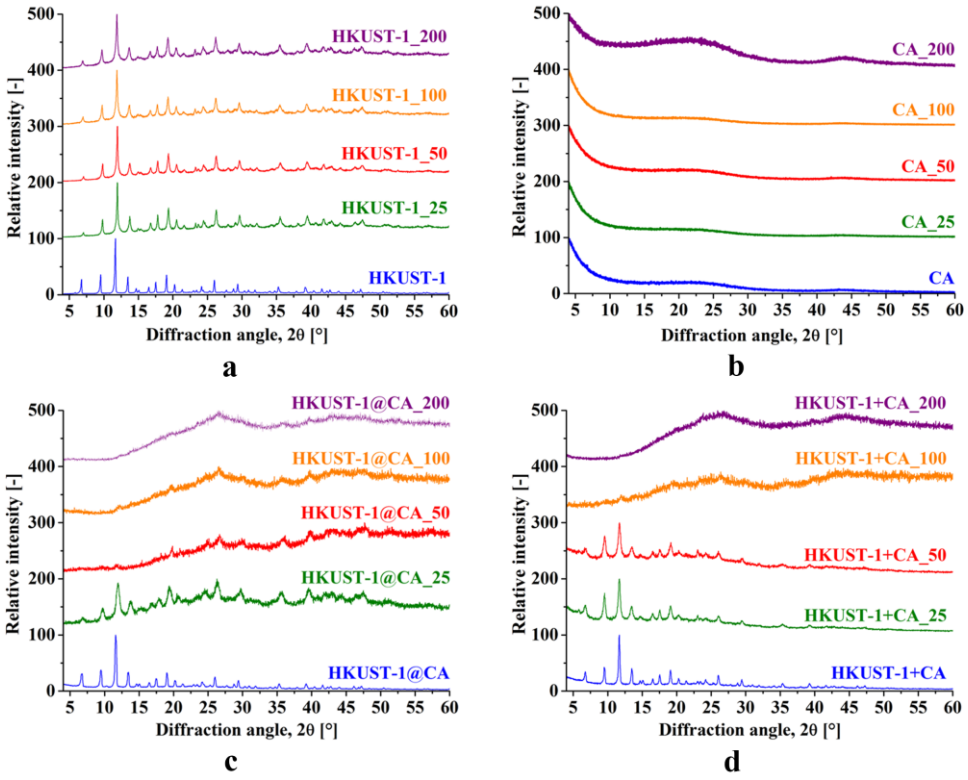

Fig. 7 Experimental XRD profile of the parent materials and the compressed samples: HKUST-1 (a) CA (b), HKUST-1@CA (c), HKUST-1+CA (d). (Each spectrum is normalized with respect to its highest count (100%).

3.2.2. Changes in the porous structure

The SEM images compare the influence of the external pressure on the 25 and 200 bar samples (Fig. 8). While only fragmentation can be observed in CA, the internal surface of the broken pellet reveals densification of the MOF. The expected protective function of the CA is obvious on comparing the images of the compressed HKUST-1 with the composite samples. The loose structure is retained in the binary systems while a layered structure develops at the higher pressure.

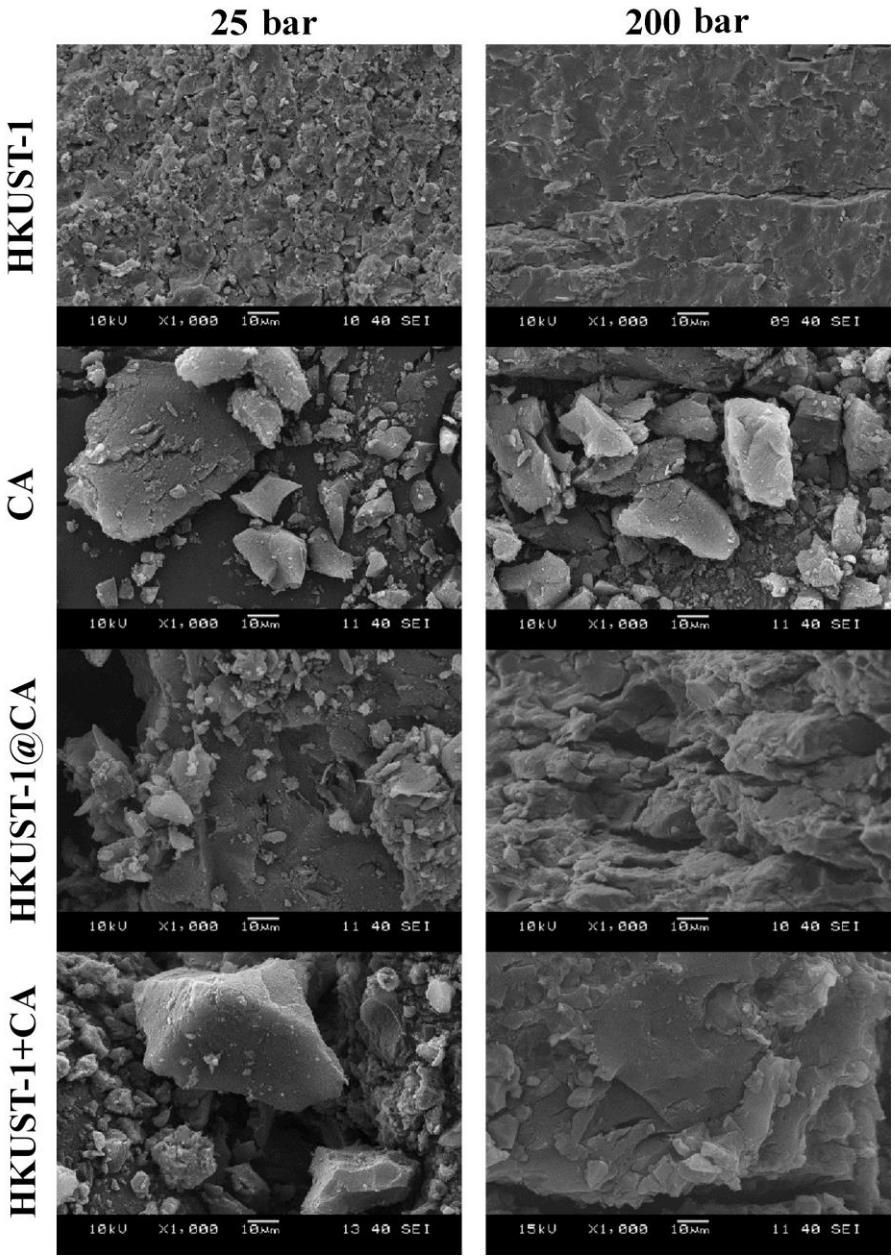

Fig. 8 SEM image of the internal surface of the various samples compressed at 25 and 200 bar

The effect of the pressure induces nanoscale changes and thus influences the adsorption properties. In the pure HKUST-1 already the smallest compression investigated causes significant changes, and further compression systematically diminishes the N_2 adsorption isotherms (Fig. 9a). The fundamental loss in gas adsorption performance stems from changes in the micropore range (Fig. S1). Additionally, a hysteresis loop of type H4 indicates the formation of slit-like mesopores. The development of mesopores was already observed when commercial HKUST-1 was subjected to pressures between 70 and 700 bar [12]. Interestingly, in that case S_{BET} decreased by 47 % at 700 bar, while here, already at 200 bar, the loss is even greater, 64 % (Fig. S1). Other studies, however, did not detect such mesopore formation [4, 18, 20]. The free volume between the individual crystals diminishes and the probes become more condensed. The reason for the mesopore evolution could be partial degradation of the isoreticular structure, which also reduces the crystallinity, as revealed by XRD.

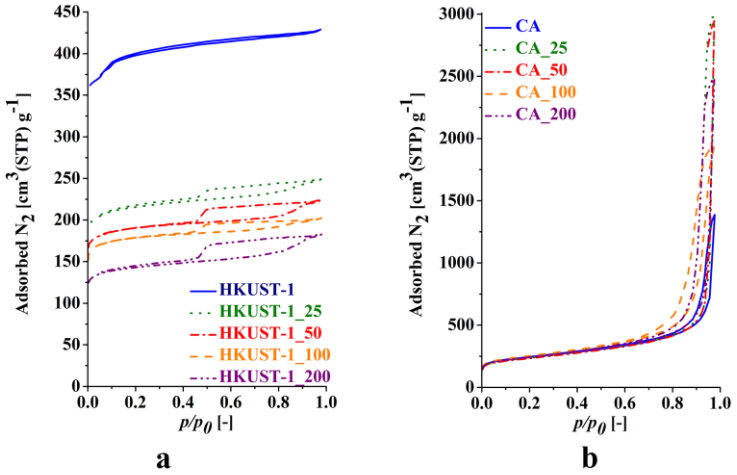

Fig. 9 Low temperature (-196 °C) nitrogen adsorption isotherms of the compressed HKUST-1 (a) and CA samples (b)

Various porous carbons of different forms and origin [18, 19, 20] are known for their high pressure resistance. Our aerogel however shows deviation in the high relative pressure range, which corresponds to wider meso- and narrow macropores: mechanical stress affects the wider pores (Fig. 9b). Interparticle spaces that exceed the window of nitrogen adsorption shrink and shift into the range already detectable by low temperature nitrogen adsorption measurements. The isotherms of HKUST-1@CA show a gradually decreasing trend similar to HKUST-1 through the whole relative pressure range (Fig. 10). The pore size distribution (Fig. 10b) reveals how mesopores narrow and their volume decreases with increasing compression. The HKUST-1+CA isotherms reveal a slightly different pressure sensitivity (Fig 11b). Up to 25 bar HKUST-1@CA seems to be more resistant, but the XRD results show that at 50 bar this obstacle disappears (Fig. 11b).

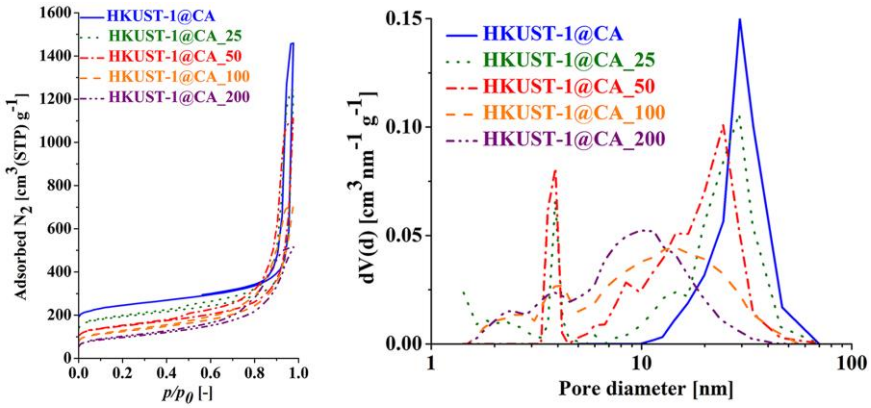

Fig. 10 Low temperature (-196 °C) nitrogen adsorption isotherms of parent and compressed HKUST-1@CA samples (a) and their pore size distributions from desorption isotherms (b)

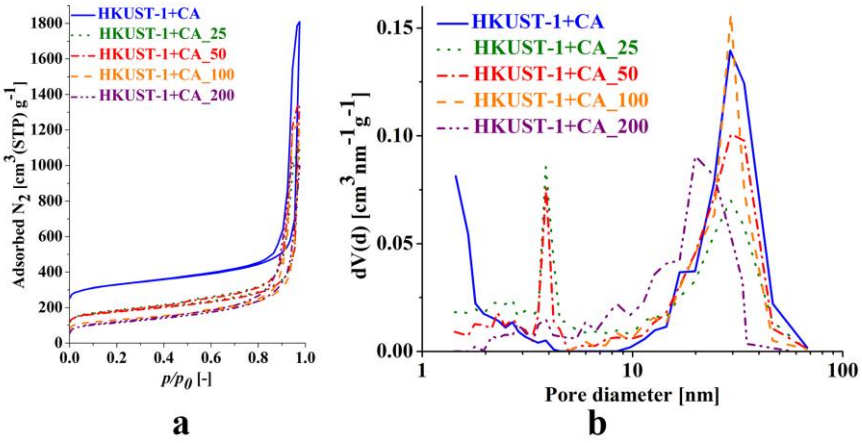

Fig. 11 Low temperature (-196 °C) nitrogen adsorption isotherms of parent and compressed HKUST-1+CA samples (a) and their pore size distributions from desorption isotherms (b)

Figure S1 and Table S2 compares the trend of the numerical parameters deduced from the nitrogen adsorption measurements of compressed samples. Not surprisingly, the apparent surface and the micropore volume shows the same tendency. It is clear that CA is the most resistant in the narrow pore region, but its structure cracks easily and the size of the voluminous wider pores shifts into the measurable pore size range, resulting in an increase in total pore volume of more than 200 %. The protective effect of the carbon is similar in both binary systems.

Methane adsorption

For applications, it is of primary importance to see the effect of the pelletization on methane adsorption capacity. Here we focus on the low pressure range. In Figure 12 we compare the methane isotherms of the various samples, as prepared and after being exposed to 100 bar. All the isotherms reflect reversible adsorption.

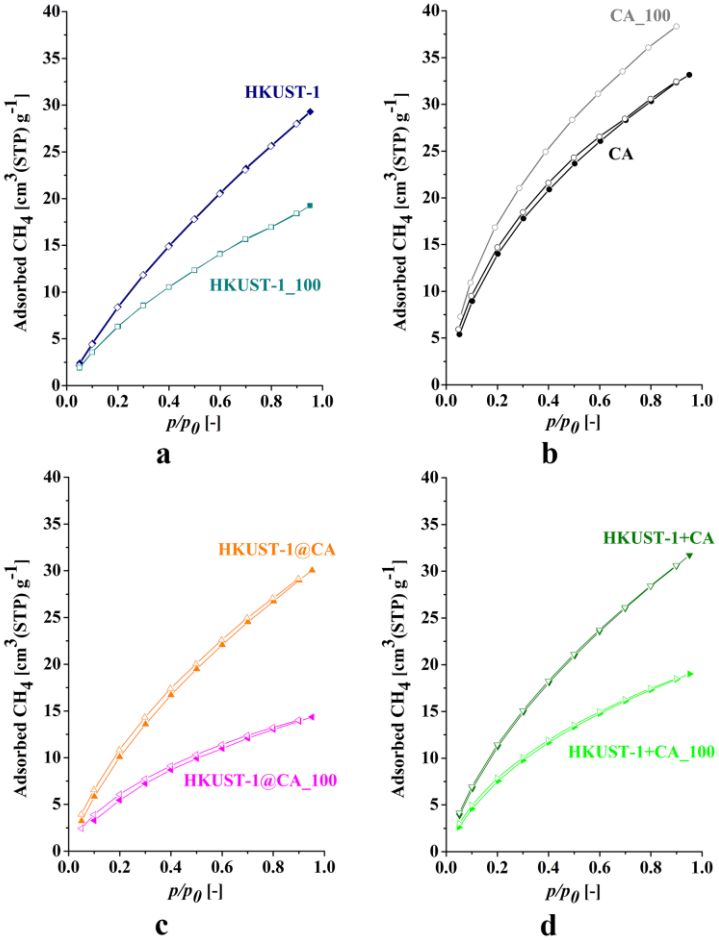

Fig. 12 Methane adsorption isotherms (0 °C, 0 - 1 bar) of HKUST-1 (a), CA (b), HKUST-1@CA (c), HKUST-1+CA (d); filled symbols: adsorption, open symbols: desorption

It is obvious that, due to the ambient test conditions applied, the capacities are significantly below the nitrogen adsorption data. The apparent advantage of CA in gravimetric terms (Fig. 12b) immediately disappears in the volumetric comparison. Owing to extremely low bulk density of CA (0.075 g cm^{-3} [48]), HKUST-1 (bulk density: 0.33 g cm^{-3}) has more than 4 times larger CH_4 capacity at atmospheric pressure than CA. The bulk densities of the HKUST-1@CA and the HKUST-1+CA composite samples were measured 0.19 g cm^{-3} and 0.12 g cm^{-3}, respectively. The corresponding adsorption capacities exceed that of the plain CA by factors of 3.5 and 2.5, respectively.

Table 3. Data deduced from methane adsorption measurements (0 °C) of non-compressed and compressed (100 bar) samples

Sample	$V_{tot,CH4}$ $cm^3\ g^{-1}$	$V_{tot,CH4\ theoretical}$* $cm^3\ g^{-1}$	Slope from DR modell
HKUST-1	0.050	X	- 0.57
HKUST-1_100	0.030	X	- 0.43
CA	0.056	X	- 0.41
CA_100	0.066	X	- 0.38
HKUST-1@CA	0.051	0.053	- 0.50

HKUST-1@CA_100	0.022	0.047	- 0.47
HKUST-1+CA	0.054	0.053	- 0.48
HKUST-1+CA_100	0.029	0.048	- 0.37

*the same calculation as for N_2 adsorption; liquid CH_4 density: 0.42 g cm^{-3}

We use the mass related adsorption data to evaluate the effect of compression on the composite samples. After compression at 100 bar the loss of CH_4 capacity was 40 % in the case of HKUST-1, 57 % for HKUST-1@CA and slightly less, 46 % for HKUST-1+CA, i.e., in the "pelletized" samples the adsorption of the HKUST-1 component governs the uptake. The trend of the additivity (or its absence) of the highest adsorption capacities is the same as in nitrogen adsorption.

The initial section of the methane adsorption isotherms were fitted to the DR model in order to estimate the effect of pressure on the adsorption energy. The slope reported in Table 3 is inversely proportional to the adsorption energy. After compression, the slopes decreased in each case, which means an enhancement of the adsorption energy. Nevertheless, the enhancement is close to 25 % in case of the pure HKUST-1 and only 7 % for CA. HKUST-1+CA behaves similarly to HKUST-1, while HKUST-1@CA shows an effect comparable to the pure CA.

4. Conclusions

Although HKUST-1 is an outstanding candidate for natural gas storage in terms of its methane uptake, it is sensitive to water and, when pelletized, to the compacting pressure. The protective effect of a carbon aerogel support was compared on two different hybrid forms of identical, 1:1 HKUST-1:CA mass ratio. HKUST-1+CA is a physical mixture, while in HKUST-1@CA the MOF crystals were grown on CA under solvothermal conditions. The effect of water vapour and the external pressure (25 - 200 bar) was investigated.

Although the XPS results imply that there is no chemical bond between the CA matrix and the MOF, the TG/DTG data show that the prehistory of the samples has a strong influence on their thermal behaviour. Moderate differences found also in the nitrogen data suggest that part of the MOF occupies the wider pores in the HKUST-1@CA sample. Although there are no dramatic differences in the water adsorption isotherms, the protective effect of the physical mixture is slightly more advantageous.

Surprisingly, the crystalline structure of HKUST-1 is well conserved when the dry powder is compressed. In this case the crystalline water lost under external pressure can be easily regained, while in the presence of the CA support this process may be hindered by the loss of water already adsorbed in the carbon pores.

The nanoscale structure of HKUST-1 + CA is more sensitive to external pressure, but at higher compressions HKUST-1 loses its crystalline structure also in the composite sample. In both cases the formation of mesopores of wide size distribution occurs. No significant difference was found between the corresponding CH_4 adsorption isotherms of the composites either in the as-prepared samples or after compression at 100 bar. After exposure to high external pressure the CH_4 uptake seems to be governed by the MOF.

Funding

This work was supported by the Hungarian grant OTKA (NN110209) and the CONCERT-EN-046 NASEMS (EU-JAPAN) project.

Acknowledgement

Support of CONCERT JAPAN (NASEMS) and OTKA (NN110209) is gratefully acknowledged. We express our gratitude to Mr. A. Farkas, Mr. T. Igricz, Mr. G. B. Pinke and Mr. Gy. Bosznai for their technical support.

References

[1] J.A. Mason, M. Veenstra, J.R. Long, Evaluating metal–organic frameworks for natural gas storage, Chem. Sci. 5 (2014) 32-51.
[2] F.-X. Coudert, A.H. Fuchs, Computational characterization and prediction of metal–organic framework properties, Coord. Chem. Rev. 307 (2016) 211-236.
[3] T.R. Zeitler, M.D. Allendorf, J.A. Greathouse, Grand Canonical Monte Carlo Simulation of Low-Pressure Methane Adsorption in Nanoporous Framework Materials for Sensing Applications, J. Phys. Chem. C 116 (2012) 3492–3502.
[4] Y. Peng, V. Krungleviciute, I. Eryazici, J.T. Hupp, O.K. Farha, T. Yildirim, Methane Storage in Metal−Organic Frameworks: Current Records, Surprise Findings, and Challenges, J. Am. Chem. Soc. 135 (2013) 11887−11894.
[5] S.S.-Y. Chui, S.M.-F. Lo, J.P.H. Charmant, A.G. Orpen, I.D. Williams, A Chemically Functionalizable Nanoporous Material $[Cu_3(TMA)_2(H2O)_3]_n$, Science 283 (1999) 1148–1150.
[6] F.-X. Coudert, Responsive Metal−Organic Frameworks and Framework Materials: Under Pressure, Taking the Heat, in the Spotlight, with Friends, Chem. Mater. 27 (2015) 1905−1916.
[7] F.-X. Coudert, Metal–organic frameworks: the pressure is on, Acta Cryst. B71 (2015) 585–586.
[8] J.C. Tan, A.K. Cheetham, Mechanical properties of hybrid inorganic organic framework materials: establishing fundamental structure–property relationships, Chem. Soc. Rev. 40 (2011) 1059–1080.
[9] K.W. Chapman, G.J. Halder, P.J. Chupas: Guest-Dependent High Pressure Phenomena in a Nanoporous Metal-Organic Framework Material: J. AM. CHEM. SOC. 130 (2008) 10524–10526.
[10] A.J. Graham, J.-C. Tan, D.R. Allan, S.A. Moggach, The effect of pressure on Cu-btc: framework compression vs. guest inclusion, Chem. Commun. 48 (2012) 1535–1537.
[11] D. Bazer-Bachi, L. Assié, V. Lecocq, B. Harbuzaru, V. Falk: Towards industrial use of metal-organic framework: Impact of shaping on the MOF properties, Powder Technology 255 (2014) 52-59.
[12] G.W. Peterson, J.B. DeCoste, T.G. Glover, Y. Huang, H. Jasuja, K.S. Walton, Effects of pelletization pressure on the physical and chemical properties of the metal–organic frameworks $Cu_3(BTC)_2$ and UiO-66, Microporous and Mesoporous Materials 179 (2013) 48–53.
[13] NaturalGas.org. http://naturalgas.org/overview/background/ (accessed 18. 07. 17.)
[14] J.J. Low, A.I. Benin, P. Jakubczak, J.F. Abrahamian, S.A. Faheem, R.R. Willis, Virtual High Throughput Screening Confirmed Experimentally: Porous Coordination Polymer Hydration, J. Am. Chem. Soc. 131 (2009) 15834–15842.
[15] P. Küsgens, M. Rose, I. Senkovska, H. Fröde, A. Henschel, S. Siegle, S. Kaskel: Characterization of metal-organic frameworks by water adsorption, Microporous and Mesoporous Materials 120 (2009) 325-330.
[16] J.B. DeCoste, G.W. Peterson, B.J. Schindler, K.L. Killops, M.A. Browe, J.J. Mahle, The effect of water adsorption on the structure of the carboxylate containing metal–organic frameworks Cu-BTC, Mg-MOF-74, and UiO-66, J. Mater. Chem. A. 1 (2013) 11922-11932.
[17] C. Petit, T.J. Bandosz, Engineering the surface of a new class of adsorbents: Metal–organic framework/graphite oxide composites, Journal of Colloid and Interface Science 447 (2015) 139–151.
[18] M.E. Casco, M. Martínez-Escandell, E. Gadea-Ramos, K. Kaneko, J. Silvestre-Albero, F. Rodríguez-Reinoso, High-Pressure Methane Storage in Porous Materials: Are Carbon Materials in the Pole Position?, Chem. Mater. 27 (2015) 959−964.
[19] J. Alcańiz-Monge, G. Trautwein, M. Pérez-Cadenas, M.C. Román-Martínez, Effects of compression on the textural properties of porous solids, Microporous and Mesoporous Materials 126 (2009) 291–301.
[20] M.E. Casco, J. Fernández-Catalá, M. Martínez-Escandell, F. Rodríguez-Reinoso, E.V. Ramos-Fernández, J. Silvestre-Albero, Improved mechanical stability of HKUST-1 in confined nanospace, Chem. Commun. 51 (2015) 14191-14194.
[21] J. Shen, Y.G. Dayong, "Preparation and Application of Carbon Aerogels," in: A.M. Aegerter, N. Leventis, M.M. Koebel (Eds.), Aerogels Handbook, Springer, New York, 2011, pp. 813–831.
[22] C. Moreno-Castilla , F.J. Maldonado-Hódar, Carbon aerogels for catalysis applications: an overview, Carbon 43 (2005) 455–465.
[23] B. Nagy, D. Ábrahám, G. Dobos, J. Madarász, G. Onyestyák, G. Sárfán, E. Geissler, K. László, Molybdenum doped carbon aerogels with catalytic potential, Carbon 66 (2014) 210-218.
[24] D. Ábrahám, B. Nagy, G. Dobos, J. Madarász, G. Onyestyák, M. V. Trenikhin, K. László, Hydroconversion of acetic acid over carbon aerogel supported molybdenum catalyst, Microporous and Mesoporous Materials 190 (2014) 46-53.

[25] O. Czakkel, E. Geissler, I.M. Szilágyi, K. László, TiO_2-doped resorcinol–formaldehyde (RF) polymer and carbon gels with photocatalytic activity, Nanomaterials and the Environment 1 (2013) 23-30.
[26] X. Xia, X. Zhang, S. Yi, H. Liu, Y. Chen, H. Chen, L. Yang, Y. He, Preparation of high specific surface area composite carbon cryogels from self-assembly of graphene oxide and resorcinol monomers for supercapacitors, J Solid State Electrochem 20 (2016) 1793-1802.
[27] M. Haghgoo, A.A. Yousefi, M.J.Z. Mehr, A. Celzard, V. Fierro, A. Léonard, N. Job, Characterization of multi-walled carbon nanotube dispersion in resorcinol–formaldehyde aerogels, Microporous Mesoporous Materials 190 (2014) 46-53.
[28] Y. Tao, D. Noguchi , C. Yang , H. Kanoh, H. Tanaka , M. Yudasaka , S Iijima, K. Kaneko, Conductive and Mesoporous Single-Wall Carbon Nanohorn/Organic Aerogel Composites, Langmuir 23 (2007) 9155-9157.
[29] S. Dong, N. Li, G. Suo, T. Huang, Inorganic/Organic Doped Carbon Aerogels As Biosensing Materials for the Detection of Hydrogen Peroxide, Anal. Chem. 85 (2013) 11739-11746.
[30] A. Dumitru, A. Morozan, M. Ghiurea, K. Scott, S. Vulpe1, Biofilm growth from wastewater on MWNTs and carbon aerogels, Phys. Stat. Sol. A 205 (2008) 1484-1487.
[31] R.W. Pekala, Organic aerogels from the polycondensation of resorcinol with formaldehyde, J. Mater. Sci. 24 (1989) 3221-3227.
[32] O. Czakkel, K. Marthi, E. Geissler, K. László, Influence of drying on the morphology of resorcinol–formaldehyde-based carbon gels, Microporous and Mesoporous Materials 86 (2005) 124–133.
[33] F. Wang, H. Guo, Y. Chai, Y. Li, C. Liu, The controlled regulation of morphology and size of HKUST-1 by ‘‘coordination modulation method’’, Microporous and Mesoporous Materials 173 (2013) 181–188.
[34] A. Domán, J. Madarász, K. László, In situ evolved gas analysis assisted thermogravimetric (TG-FTIR and TG/DTA–MS) studies on non-activated copper benzene-1,3,5-tricarboxylate, Thermochimica Acta 647 (2017) 62–69.
[35] F.H. Allen, The Cambridge structural database: a quarter of a million crystal structures and rising, Acta Cryst. B58 (2002) 380–388.
[36] C.F. Macrae, I.J. Bruno, J.A. Chisholm, P.R. Edgington, P. McCabe, E. Pidcock, L. Rodriguez-Monge, R. Taylor, J. van de Streek, P.A. Wood, Mercury CSD 20-new features for the visualization and investigation of crystal structures, J. Appl. Cryst. 41 (2008) 466–470.
[37] S. Brunauer, P. Emmett, E. Teller, Adsorption of gases in multimolecular layers, J. Am. Chem. Soc. 60 (1938) 309–319.
[38] M.M. Dubinin, L.V. Radushkevich, Equation of the characteristic curve of activated charcoal, Chem. Zentr. 1 (1) (1947) 875.
[39] E.P. Barret, L.G. Joyner, P.H. Halenda, The Determination of Pore Volume and Area Distributions in Porous Substances. I. Computations from Nitrogen Isotherms, J. Am. Chem. Soc., 73 (1951), 373-380.
[40] G. Majano, O. Martin, M. Hammes, S. Smeets, C. Baerlocher, J. Pérez-Ramírez, Solvent-mediated reconstruction of the metal-organic framework HKUST-1 ($Cu_3(BTC)_2$), Adv. Funct. Mater. 24 (2014) 3855–3865.
[41] CSD refcode FIQCEN, Experimental Crystal Structure Determination by S.S.-Y.Chui, S.M.-F.Lo, J.P.H. Charmant, A.G. Orpen, I.D. Williams Deposited on: 4/1/1999, CCDC: 112954.
[42] CSD refcode DOTSOV42, Experimental Crystal Structure Determination through neutron diffraction by S. Xiang, W. Zhou, J.M. Gallegos, Y. Liu, B. Chen, (J. Am. Chem. Soc., 2009, 131, 12415-12419). Deposited on 17/11/2009, CCDC: 755080.
[43] PDF 00-062-1183, Copper benzene-1,3,5-tricarboxylate trihydrate (copper trimesate trihydrate, $Cu_3(C_9H_3O_6)_2•3H_2O$). Prepared by mechanosynthesis from copper nitrate and benzene-1, 3, 5-tricarboxylic acid precursors by Audebrand, N., Univ. de Rennes I, Laboratoire Sciences Chimiques de Rennes, France., ICDD Grant-in-Aid, (2011).
[44] PDF 00-064-0936, Bis(benzene-1,3,5-tricarboxylato)tricopper(II) hydrate (Basolite C300), $Cu_3((O_2C)_3C_6H_3)_2·9.4H_2O$. Commercial material, prepared by BASF and purchased from Sigma-Aldrich. Pattern measured in equilibriumwith the atmosphere. The initially dehydrated material absorbed water fromthe atmosphere. Kaduk, J., Poly Crystallography Inc., Naperville, IL, USA;Wong-Ng, W., NIST, Gaithersburg, MD, USA., ICDD Grant-in-Aid, (2012).
[45] PDF 00-065-1028, Copper benzene-1,3,5-tricarboxylate (Basolite C300; Cu-BTC MOF; HKUST-1, Purchased commercial material (Lot STBC4614 V)),$Cu_3((O_2C)_3C_6H_3)_2$. Sample was dehydrated at 423 K overnight under vacuum. Pattern measured at beam line 11-BM, (goniometer radius 1000 mm) Advanced Photon Source, Argonne National Laboratory, Lement, Illinois,USA. Data collected using Debye-Scherrer geometry. Kaduk, J., PolyCrystallography Inc., Naperville, IL, USA., ICDD Grant-in-Aid, (2014).
[46] F. Rouquerol, J. Rouquerol, K.S.W. Sing, P. Llewellyn, G. Maurin, Adsorption by Powders and Porous Solids Principles, Methodology and Applications, second ed., Academic Press, 2014.
[47] Sigma-Aldrich®. http://www.sigmaaldrich.com/catalog/product/aldrich/688614?lang=hu&region=HU (accessed 18. 07. 17.)

[48] B. Nagy, A. Tóth, I. Savina, S. Mikhalovsky, L. Mikhalovska, I. Grillo, E. Geissler, K. László, Small angle neutron scattering study of globular proteins confined in porous carbons, Carbon 106 (2016) 142-51.